

“Stainless Uranium” - Oxidation Prevention in Uranium-Niobium Alloys

Logan Coleman Page

A thesis submitted to the faculty of

Brigham Young University

In partial fulfillment of the requirements for the degree of

Bachelor of Science

Dr. David D. Allred, Advisor

Department of Physics and Astronomy

Brigham Young University

April 2021

Copyright © 2021 Logan Coleman Page

All Rights Reserved

ABSTRACT

“Stainless Uranium” - Oxidation Prevention in Uranium-niobium Alloys

Logan Coleman Page

Department of Physics and Astronomy

Bachelor of Science

Uranium, a nuclear fuel source, can oxidize and degrade in reactor conditions. Previous studies have shown oxidation resistance in a uranium-niobium alloy. The nature of the oxides that form on U-6Nb after long exposure to air was explored using neutron diffraction at Los Alamos National Laboratory. We deposited thin films of uranium-niobium alloys for oxidation studies. We used ellipsometry to quantify the oxide growth over time as a function of niobium content. We found that the oxide thickness increases linearly with the logarithmic of time. This study also supports the hypothesis that uranium and niobium oxides form a protective passivation layer on a uranium alloy, preventing oxidation and extending the life of the fuel.

Keywords: Uranium; Niobium; Alloy; Passivation; Stainless; Oxidation; Nuclear Fuel; Uranium Oxide; Ellipsometry; Fuel Rod Degradation

Acknowledgments

For their excellent undergraduate research program of which I am a part, I thank the Department of Physics and Astronomy at Brigham Young University. I am also grateful to my research advisor, Dr. David Allred, for his immense expertise and patience as he guided this research and the writing of this thesis.

I would like to thank Erik Watkins and Jaroslaw Majewski at Los Alamos National Laboratory for their collaboration on this project. I also thank Josh Vawdrey, Kenan Fronk, and others in Dr. Allred's research group at BYU for their contributions to this project.

Table of Contents

List of Figures	5
List of Tables	5
List of Equations	5
1 Introduction	6
1.1 Motivation	6
1.2 Oxidation Resistance	6
1.3 Current Work	7
2 Methods	8
2.1 Sample Selection	8
2.2 Sample Preparation	8
2.3 Sample Characterization	11
2.3.1 Energy Dispersive X-Ray Spectroscopy (EDX)	11
2.3.2 Ellipsometry	13
3 Results and Discussion	15
3.1 Sample Composition	15
3.2 Ellipsometric Thickness of Samples	16
4 Summary and Conclusions	20
4.1 Implications	20
4.2 Future Work	20
Appendix A	21
A.1 Stepper Motor Controller Design with Phidget®	21
A.2 PyInstaller Setup File	24
Index	26
Bibliography	27

List of Figures

Fig 1 - Long-term oxide structure.....	7
Fig 2 - Sputter deposition.....	9
Fig 3 - Uranium-niobium target configuration.	10
Fig 4 - Example energies of characteristic x rays	12
Fig 5 - Ellipsometry	14
Fig 6 - EDX spectrum of UNb film	15
Fig 7 - Oxide layer thickness over time	17
Fig 8 - Uranium oxide layer.....	18
Fig 9 - Niobium oxide layer.....	19
Fig 10 - UNb alloy	19

List of Tables

Tab 1 - EDX Composition	16
Tab 2 - Thickness over time.....	16
Tab 3 - Fit parameters	18

List of Equations

Eq 1 - Kanaya-Okayama Range Equation	13
Eq 2 - Logarithmic growth model.....	17

1 Introduction

1.1 Motivation

Many nuclear fission power plants around the world use uranium (U) fuel. However, uranium fuel rods can oxidize rapidly in working ambient conditions. [1] Over time, oxidation can permeate through the entire volume of the rod. The resulting uranium oxide phases (UO_x) have an increased volume compared to pure U. This expansion can cause cracks and swelling in the volume of the fuel rod. Thus, oxidation advances corrosion. [2]

1.2 Oxidation Resistance

A variety of corrosion-resistant alloys, referred to as “stainless uranium”, have been found through the addition of elements such as niobium, molybdenum, and zirconium. [3] In the present study, we focus on uranium-niobium (U-Nb) alloys. These alloys can be compared to stainless steel because of the passive oxide layer that forms on the surface of the alloy.

Stainless steel consists of iron (Fe) enriched with various elements, including more than 11% chromium, in a passivating oxide layer which is tens of nanometers thick, composed of chromium oxide (Cr_2O_3) on top of iron oxide. [5] The Cr_2O_3 layer retards the entry of more oxygen into the metal, thus slowing further corrosion and giving the steel its “stainless” quality. If the oxide layer is damaged or removed, it will simply reform as the newly revealed surface oxidizes. Thus, the passivation layer is self-healing. [6]

As with stainless steel, a passive oxide layer can form on U-Nb alloys significantly slowing the oxidation process, creating a type of “stainless uranium”. So far, few studies have characterized the formation of the passivating oxide layers in U-Nb. [3,4,8,9] Analysis of the Gibbs enthalpy of oxidation in stainless steel and stainless uranium has shown that while

stainless steel favors a Cr_2O_3 surface on top of iron oxide, stainless uranium instead forms UO_x on the surface, leaving an Nb-enriched area underneath to oxidize and provide a passivating barrier. [7,10]

Experimental observation of the nature of these oxides had been inconclusive, with some studies indicating an intermixed UO_2 - Nb_2O_5 oxide providing a critical Nb_2O_5 density, and others indicating chemical segregation of the UO_2 and Nb_2O_5 layers. [8,9] A recent publication by Watkins, et al. from Los Alamos National Laboratory found an interesting layer formation in U-Nb thin films via neutron reflectometry and x-ray reflectometry. They demonstrated the long-term behavior of the passive oxide layers, finding a 31 nm thick UO_2 layer on top of a laterally undulating 5 nm Nb_2O_5 layer as shown in Fig. 1. These oxide layers created a stable equilibrium in which the underlying U-Nb alloy was not oxidized. [10]

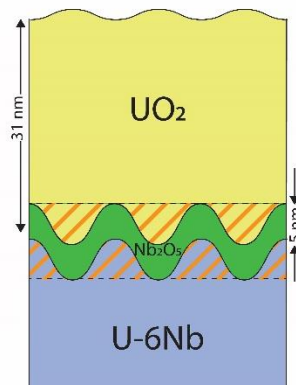


Fig 1 - The long-term oxide layer structure as observed by Watkins, et al. [9]

1.3 Current Work

Here, I expand upon the previous literature by investigating the formation over time of the oxide layers in a uranium-niobium alloy. After sputter-depositing a satisfactory U-Nb thin film, ellipsometry was the primary characterization tool. I intended to investigate the growth pattern of the separated oxide layers over time.

2 Methods

2.1 Sample Selection

To observe the oxidation of the alloy over time, we deposited U-Nb thin films on silicon wafers via sputtering. Observation of new films as they aged provided data to model the alloys' oxidation over the short-term (days) and long-term (months).

Our substrates were cleaved from [100] orientation silicon test wafers coated with approximately 300 nm of chemical vapor deposition (CVD) silicon nitride on the surface. We cleaved rectangular pieces approximately 25 mm by 75 mm, to best use the space both in our sputtering chamber and our storage containers. Previous work in Dr. Allred's research group shows these wafers to have approximately 0.1 nm RMS roughness over a 1 micron by 1 micron surface.

2.2 Sample Preparation

To prepare thin films of uranium-niobium, we used a DC-magnetron vacuum sputtering system. DC-magnetron sputtering is a physical vapor deposition (PVD) process that uses a vacuum environment to deposit thin films atom by atom. In the example shown in Fig. 2, the sputter gun is at the bottom of the vacuum chamber in "sputter up" geometry. Above the sputter gun, a substrate is placed to receive the deposited film. "Sputter up" indicates that uranium atoms are knocked out of the source at the bottom of the chamber and travel upwards towards the substrate above. The source is a thin, circular uranium plate, or target, in electrical and thermal contact with the sputter gun's high voltage cable.

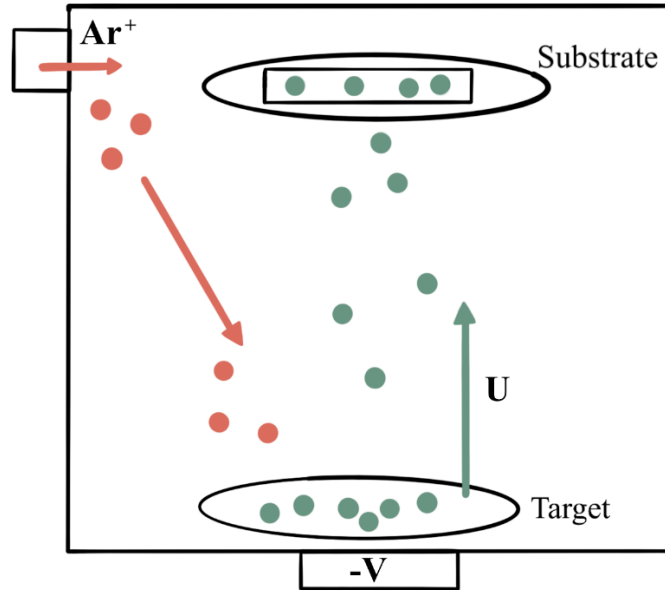
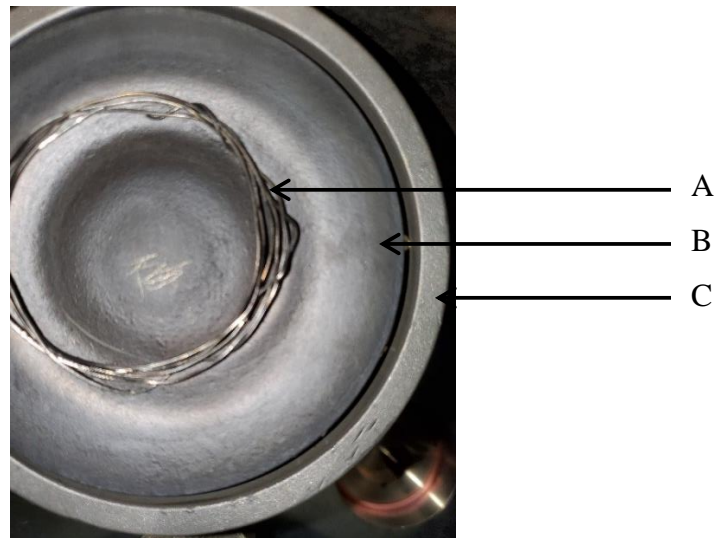


Fig 2 – Sputtering deposition process - In the sputtering deposition process, argon gas is ionized and accelerated toward the uranium target. Uranium and niobium particles are released from the target and contact the substrate above, forming a thin film.

With the chamber in high vacuum, an inert gas like argon—called the working gas—is introduced to bring the chamber pressure to the desired level, often in the range of 1 mTorr. The target is used as a cathode, and a highly negative DC bias is applied. At sufficient negative voltage, the argon “breaks down” to form a plasma. In the case of magnetron sputtering, this plasma is confined above the target by strong magnets underneath the target. The plasma is slightly positive, and therefore argon atoms in the plasma are attracted to the negatively biased target. These argon atoms are accelerated towards the target by the high negative voltage between the plasma and the target to relatively high energy (about 400 eV). The energetic ions produce a cascade of collisions in the surface of the target. The transfer of momentum knocks some atoms out of the target, which then fly up to the substrate and accumulate a thin film.

In our vacuum sputtering system, a Meivac MAK sputter gun was at the bottom of the vacuum chamber. A 10 cm diameter depleted uranium target (material purchased from Nuclear Fuel Services, Inc) was in electrical and thermal contact with the sputter gun. We looped

niobium wires and placed them in the target's "racetrack", the most heavily eroded section, as shown in Fig. 3. Adjusting the number of wire coils allowed us to change the ratio of niobium to uranium in the deposited films. It was earlier found that three loops of niobium wire produced a film of 6% weight niobium.[10] The substrate was fixed to the surface of a 4.5" platten which revolved as it rotated around the chamber in a planetary motion to promote uniform thickness over a large sample area, as is discussed in reference [10].



*Fig 3- A photograph of the sputtering target and wire. A: Several loops of Niobium wire placed in the racetrack.
B: Uranium target. C: Dark space shield surrounding sides of uranium target.*

The system's high vacuum pump was a turbomolecular pump. We evacuated our chamber until high vacuum was reached (< 0.1 mTorr) and impurities such as water vapor were pumped out of the system (as determined by a mass spectrometer). We then flowed in argon gas at a constant flow rate as controlled by a mass flow controller. With the turbo pump and argon flow both running, we maintained a constant pressure of about 1 mTorr as measured by a MicroPirani gauge and a 0.1 Torr Baratron. We found that the plasma was stable near 1 mTorr. While the chamber was exposed to atmosphere, some oxide tended to form on the target. To avoid depositing oxidized material in the film, we presputtered the target for several minutes to

remove oxide and other impurities. During this time, the substrate was covered by rotating it inside the chamber to lie above an unused target on the opposite side of the chamber. That target was raised close to the substrate, blocking any incident sputtered particles. Once the target was cleaned of oxides, we began rotating the substrate over the target. During sputtering, the DC power supply was set to constant power. The initial power was around 450 V and 0.30 A. As time went on, the voltage decreased to about 350 V as the current increased to 0.37 A. This indicates an increase in conductance of the system over the course of sputtering, possibly due to removal of residual surface oxide. The potential and current helped identify the cleanliness of the target, as a stable current indicated a stable resistivity and a lack of oxide. With a motor controlling the rotation of the substrate, we could vary both the rotation speed and duration. Rotating the sample at $10^\circ/\text{s}$ over the plasma for nine rotations produced a film thin enough to measure with ellipsometry. Rotating for 60 rotations at the same speed produced a film thick enough that material began to flake off.

2.3 Sample Characterization

To characterize the samples after sputtering, we used two methods: energy dispersive X-ray analysis (EDX) and ellipsometry. EDX was primarily used to determine film composition. Ellipsometry was used to measure film thickness and index of refraction, especially as those characteristics changed over time.

2.3.1 Energy Dispersive X-Ray Spectroscopy (EDX)

EDX uses the electron beam an electron microscope to bombard a sample, stimulating x-ray emission. As these electrons collide with the sample atoms, they can eject electrons in the sample from their orbits. When an atom loses a low-energy electron, one of its high-energy electrons will transition downward to fill the hole, emitting an x ray in the process. Each element

produces x rays of characteristic energies, depending on the element's electron structure. X rays emitted from a sample are matched to characteristic x rays to determine which elements are present in what quantities. An example of these characteristic x rays is given in Fig. 3, a diagram from reference [11]. Comparing the amplitude and proportion of the detected x rays allows numerical identification of component elements. We measured each film to identify the ratio of niobium to uranium.

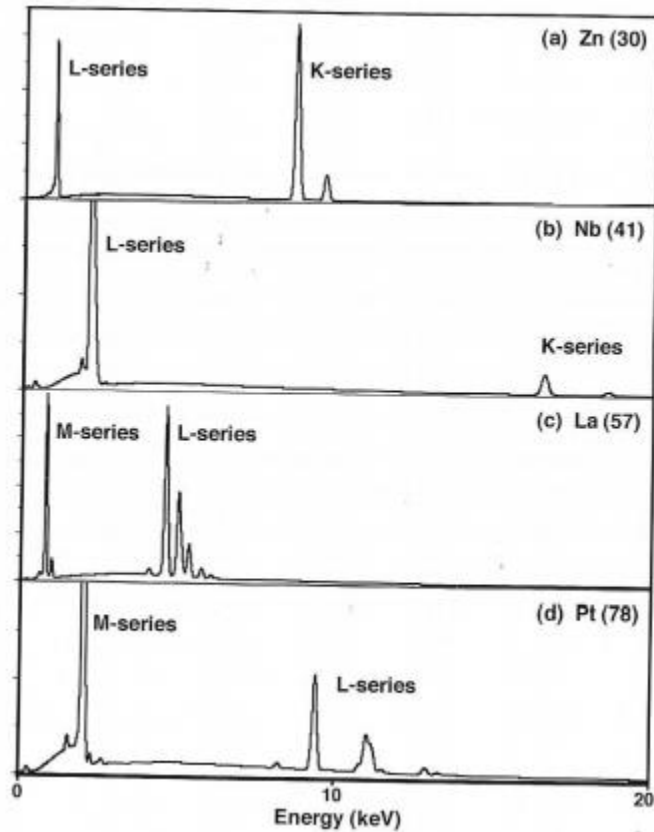


Fig 4 – A plot of the energies of characteristic x rays emitted by several example elements.

The EDX user is free to vary many parameters of the incident electron beam to tailor the signal to match the analytic task. An important optimization in my use of EDX was a low electron beam energy. A lower energy electron would only interact with a smaller volume near

the surface. A high-energy electron penetrates more deeply into the sample, and thus interacts with both a greater depth and greater area of the sample. A high-energy electron can also excite atoms to emit higher energy x rays, allowing for a greater range of characteristic x rays to be measured. Thus, beam energy constitutes a trade-off to optimize both spatial precision and spectral range. In my measurements, I used a 5 keV electron beam for an interaction depth between 89 to 161 nm, as calculated with the Kanaya-Okayama Range Equation (Eq. 1). [11]

$$R_{KO}(nm) = \frac{27.6 A}{Z^{0.89} \rho} E_0^{1.67}$$

Eq 1 - The Kanaya-Okayama Range Equation

In this equation, A is the sample's atomic weight (g/mol), Z is its atomic number, ρ is its density, and E_0 is the electron beam energy. The constant 27.6 gives results in nanometers; 0.0276 gives microns. At 5 keV, a sample of pure uranium would have a penetration depth of 89.3 nm, and pure niobium would have a depth of 161 nm. Because my samples contain primarily uranium (>90%) and are expected to be 100 nm thick, I expected a 5 keV electron beam to interact almost exclusively with the alloy, without reaching the underlying substrate. In practice, this minimized the x ray response from the underlying silicon nitride, although it did not entirely eliminate it.

2.3.2 Ellipsometry

Variable-angle spectroscopic ellipsometry (VASE) was the primary means of sample characterization. An ellipsometer measures the optical properties of a sample by measuring the change in polarization of a polarized light source after reflection at a specified angle as shown in Fig. 5. A variable-angle spectroscopic ellipsometer obtains more complete data on a sample by measuring at a series of angles over a spectrum of photon energies.

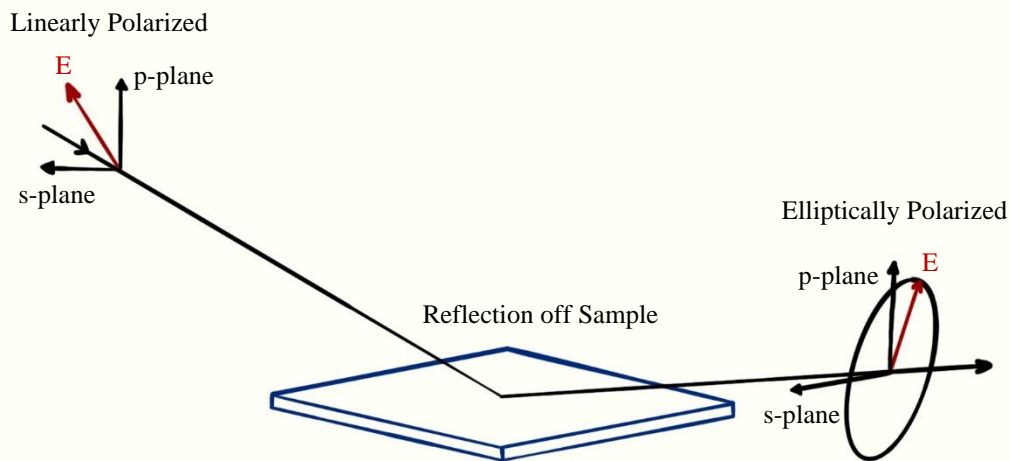


Fig 5 - Ellipsometry uses a known light source to measure the optical properties of a reflective surface.

We used a VASE ellipsometer and CompleteEASE software, both from J. A. Woollam, to measure our thin films. A key feature of the ellipsometry analysis was the interference patterns produced by the varying wavelengths of incident light at a given angle. As we produced samples, we measured them with the ellipsometer immediately after deposition. Many of the films we deposited had a metallic silver appearance and were too opaque to show thin film interference from the underlying Si_3N_4 layer. A few were purple in appearance and thin enough to permit thin film interference; our analysis focuses on one of these films.

3 Results and Discussion

3.1 Sample Composition

Within a week of deposition (depending on electron microscope availability), we performed energy dispersive x-ray analysis on fragments of the samples (stored in atmosphere) to determine composition. EDX measurements on the sample with 3 loops of Nb wire, taken 5 days after sputtering, revealed the composition shown in Table 1. The sample showed some evidence of carbon and oxygen, whose x-ray peaks overlap with uranium, confounding analysis. Any carbon present was most likely adventitious and/or deposited during the measurement process. Smaller amounts of nitrogen and silicon were also observed, indicating that the interaction volume of the microscope's electron beam exceeded the thickness of the film and passed through to the underlying Si_3N_4 layer. Since our aim is to determine the ratio of niobium to uranium in the film, we renormalized the measurements including only the niobium and uranium components.

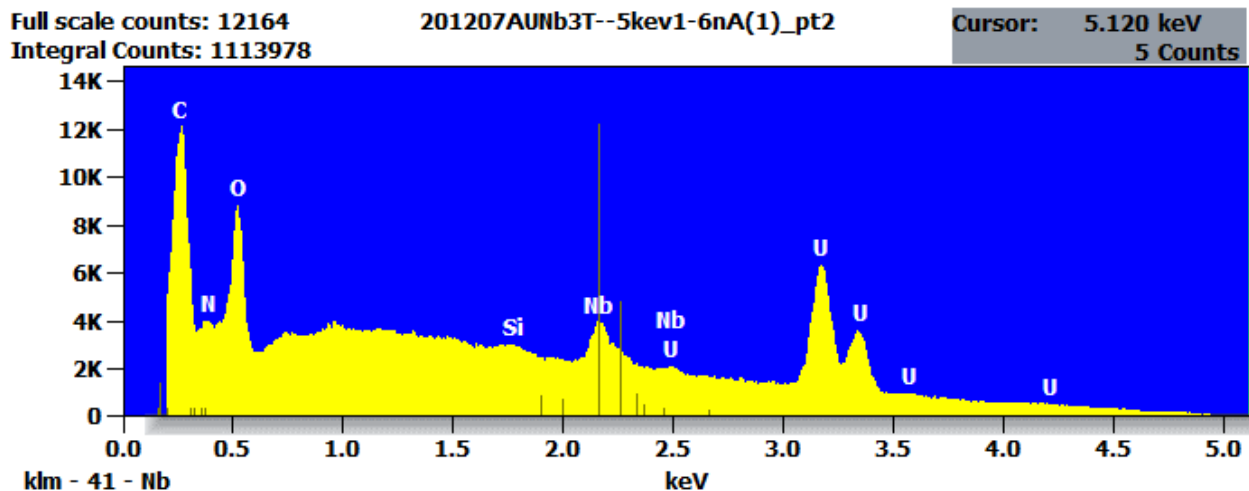


Fig 6 – EDX spectrum of the 3-loop UNb film, with a nominal ellipsometric thickness of 150 nm.

	<i>N</i>	<i>O</i>	<i>Si</i>	<i>Nb</i>	<i>U</i>
Weight %	0.74	1.30	0.23	3.80	93.10
Atomic %	8.26	12.64	1.30	6.37	60.88
Renormalized Weight %				3.92	96.08
Renormalized Atomic %				9.47	93.89

Tab 1- EDX measurements 5 days after sputtering show the sample produced from 3 loops of Nb wire to contain 3.92% weight Nb after renormalization.

3.2 Ellipsometric Thickness of Samples

This same 3-loop sample was purple in appearance and showed measurable interference fringes through measurement. This film also had a similar composition to the sample used by Watkins et al. We therefore focus our ellipsometric thickness measurements on this film.

We measured the film repeatedly at increasing intervals over the course of months. We then fit the data to an optical model representing different layers in the film. The model that best fit the data included a series of three distinct layers of uranium oxide, niobium oxide, and uranium-niobium alloy, as shown in Tab. 2 and Fig. 7, as well as an underlying 300 nm layer of silicon nitride (not shown). According to this model, the niobium oxide and uranium oxide layers grew logarithmically over time. The thicknesses estimated by this model seem too large. Other films we produced that were too opaque were also in the 100 nm thickness range, so we believe this sample to be thinner than it appears. We suspect inaccuracies in the optical constants of our model but have yet to verify this, and so we are using the 150 nm thicknesses as nominal values. The figure shows a logarithmic oxide growth, which agrees with the work of Watkins et al. in determining a long term oxide state for similar films.

Oxide Layer Thickness Over Time												
Time (mins)	80	285	500	780	1600	2160	6500	19000	38000	56000	65000	110000
UO2 Thickness (nm)	7.97	18.49	21.75	25.61	30.09	31.65	37.64	42.48	44.97	59.13	50.86	60.06
Nb2O5 Thickness (nm)	2.44	6.66	7.53	9.64	11.8	12.5	14.81	18.53	20.94	28.03	24.98	32.83
UNb Thickness (nm)	135.13	122	117.74	113.39	108.02	106.08	102.32	95.36	98.64	75.59	77.96	68.11

Tab 2 - Thickness of thin-film layers over time, as measured with ellipsometry.

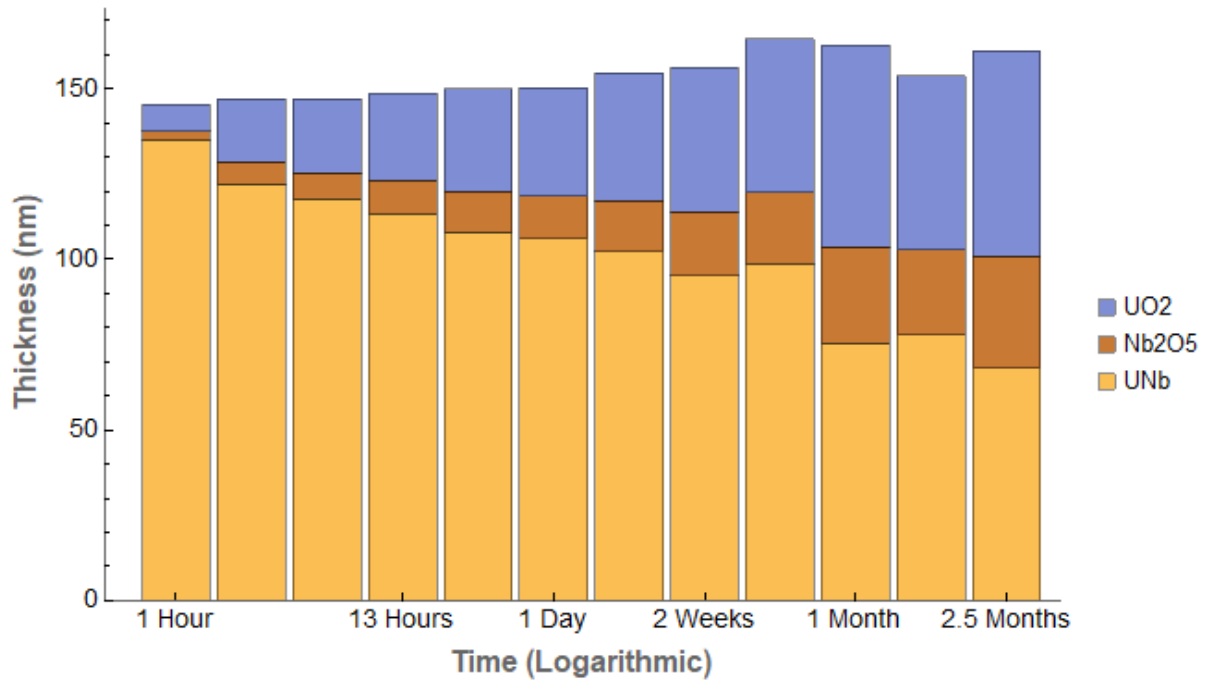


Fig 7- The oxide layers' thickness over time. UO₂ migrated to the outside; Nb₂O₅ underneath, on top of the UNb alloy.

The uranium moved outward as it oxidized. The niobium oxide grew under the uranium oxide, directly on top of the original uranium-niobium alloy. As seen in Fig. 7, the uranium oxide was much thicker than the niobium oxide; this is likely the result of the original ratio of uranium to niobium in the alloy. The oxide thickness grows logarithmically as described by Eq. 2.

$$d(t) = A \ln t + B$$

Eq 2 - The logarithmic growth model used to fit the ellipsometric data.

Fitting the thickness of each layer in the thin film to Eq. 2 provided the values shown in Tab. 3. The A values indicate, as also seen in Fig. 7, that the UO₂ layer grew nearly twice as fast as the Nb₃O₅ layer, while the combined oxide layer growth outpaced the shrinking of the underlying alloy. These model fits are displayed relative to their corresponding data points in Fig. 8, 9 and 10. The logarithmic slowing of the oxidation left the internal uranium-niobium

alloy unoxidized only tens of nanometers under the surface. This follows the expected behavior of the passivation layer, retarding the oxidation of the alloy.

	A	B
UO ₂	6.64411	-19.8992
Nb ₃ O ₅	3.74338	-15.5425
UNb	-7.96309	168.561

Tab 3 - The parameters found to best fit the oxide growth behavior to the logarithmic growth model.

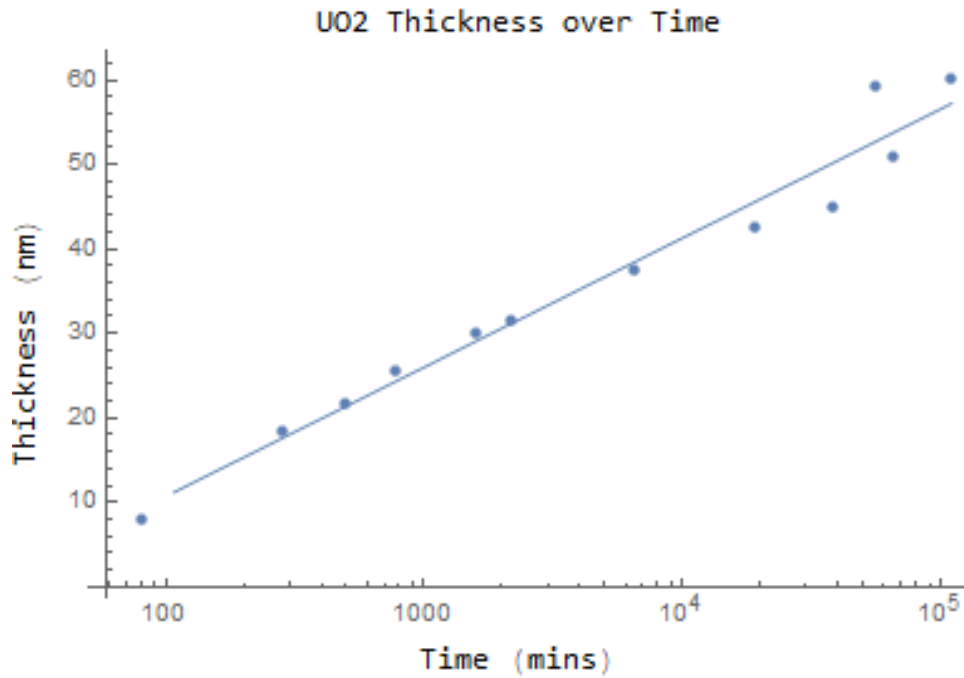


Fig 8 - Thickness of the uranium oxide layer as it formed on the outer surface of the UNb thin film.

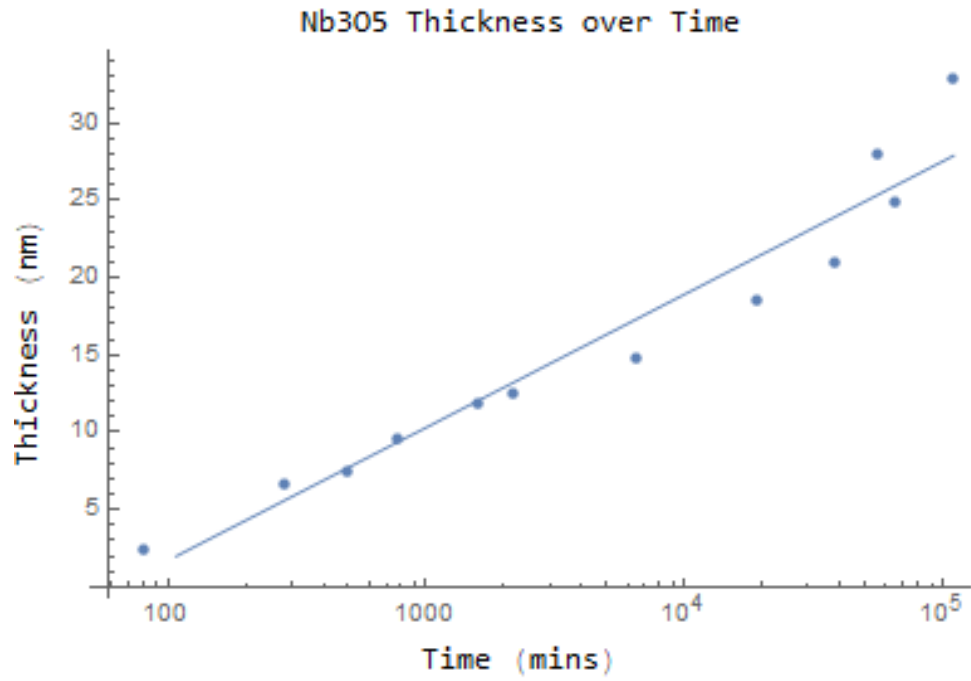


Fig 9 - Thickness of the niobium oxide layer as it formed between the uranium oxide and uranium niobium layers.

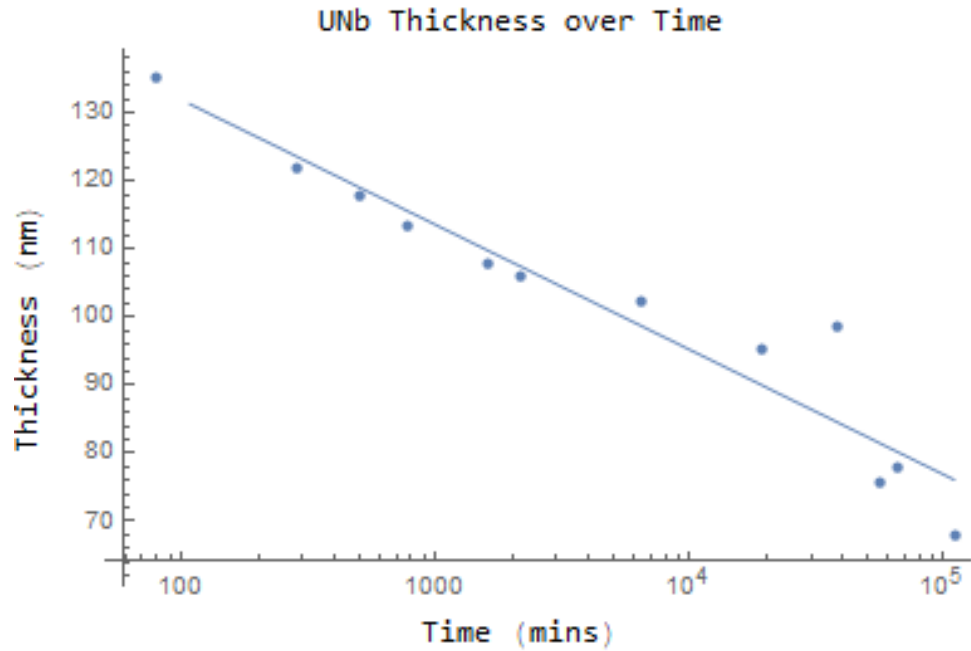


Fig 10 - Thickness of the original UNb alloy as some of its exterior was oxidized.

4 Summary and Conclusions

4.1 Implications

The observed uranium and niobium oxide layers which formed retarded the long-term oxidation of the alloy following the logarithmic law in Eq. 2. This slowing confirms the hypothesis of a passivation layer forming on “stainless uranium”. A notable difference from stainless steel was observed in our sample. As explained previously, stainless steel passivates as chromium oxide forms on the outer surface. In our alloy, the passivation layer of niobium oxide formed underneath the uranium oxide rather than on top. This indicates that the oxidation layers in stainless steel may have theoretical differences from the layers in the uranium-niobium alloy, including a different Gibbs energy as has been noted. The key result, however, is clear: since the alloy shows a slowing rate of oxidation with time, the niobium oxide is creating an oxidation-resistant passivation layer.

4.2 Future Work

Further work has begun with investigating similar oxide formation in alloys with varying proportions of niobium to uranium. It may be found that a variation in the amount of niobium increases the oxidation resistance of the alloy.

Appendix A

A.1 Stepper Motor Controller Design with Phidget®

The following is a Python program I wrote to operate the Phidget Stepper Motor Controller Model 1063_1 which rotated our substrate during sputtering. In writing, I drew from several sources including Phidget documentation, Tkinter documentation, and StackOverflow.com. The program produces a windowed Graphical User Interface (GUI) which accepts inputs for rotation speed, number of rotations, and rotation direction, and outputs the motor's actions in a text box.

```
# -*- coding: utf-8 -*-
"""
Created on Fri Sep  4 19:08:09 2020
GUI that can control the Phidget Stepper Motor
@author: Logan Page
"""
import tkinter as tk
import sys
from Phidget22.Phidget import *
from Phidget22.Devices.Stepper import *
from Phidget22.Devices.DigitalInput import *
from Phidget22.Devices.CurrentInput import *
import threading

#Print window definition
class PrintLogger(): # create file like object
    def __init__(self, textbox): # pass reference to text widget
        self.textbox = textbox # keep ref

    def write(self, text):
        self.textbox.insert(tk.END, text) # write text to textbox
        self.textbox.see(tk.END) # scroll to end of textbox to make new lines always visible

    def flush(self): # needed for file like object
        pass

def rotate():
    if stepper0.getIsMoving() == True:
        stepper0.setVelocityLimit(0)

    vel=ent_runspeed.get()
    rots=ent_rotations.get()
    direction = var_direction.get()
```

```

#check valid input
if len(vel)==0:
    print('Input desired velocity.')
    return
if len(rots)==0:
    print('Input desired rotations.')
    return

vel=int(vel)
rots=int(rots)

if direction==True:
    direct = "backward";
    int_direct=-1;
else:
    direct="forward";
    int_direct=1;

#Seconds per rotation
global rotlength
rotlength = 360/vel

#Timer for full run
global timer
timer = threading.Timer(360*rots/vel, stopRotation)

#Timer to count individual rotations
global countrotationtimer
countrotationtimer = threading.Timer(rotlength, countRotation)
global counter
counter = 0

print("Turning " + str(direct) + " at " + str(vel) + "%s for " + str(rots) + " turns.")
stepper0.setVelocityLimit(int_direct*vel)
stepper0.setEngaged(True)
timer.start()
countrotationtimer.start()

def stopRotation():
    print('Stopping')
    stepper0.setVelocityLimit(0)
    stepper0.setEngaged(False)
    global timer
    if(timer is not None):
        timer.cancel()
    global countrotationtimer
    if(countrotationtimer is not None):
        countrotationtimer.cancel()
    global counter
    counter = 0

def onAttach(self):
    print("Attached!")

```

```

def onDetach(self):
    print("Detached!")

def countRotation():
    global counter
    global countrotationtimer
    global rotlength
    counter += 1;
    print(str(counter))
    countrotationtimer.cancel()
    countrotationtimer = threading.Timer(rotlength, countRotation)
    countrotationtimer.start()

#Timer for setting rotation count
global timer
timer = None
global countrotationtimer
countrotationtimer = None
#Create a new stepper controller channel
stepper0 = Stepper()

#General Window/Frame Setup
window=tk.Tk()
window.title("Phidget Stepper Control")
window.geometry("425x400")

frm_buttons = tk.Frame(master=window)
frm_buttons.grid(row=1,column=0,sticky="nesw",padx=10,pady=10)
frm_buttons.grid_columnconfigure((0,1,2,3),weight=1) #needed for centering

frm_info = tk.Frame(master=window)
frm_info.grid(row=0,column=0,sticky="nesw", padx=10,pady=10)
frm_info.grid_columnconfigure((0,1,2,3),weight=1) #needed for centering

#Establish input options
lbl_runspeed = tk.Label(master=frm_info, text = "Degrees/sec: ")
ent_runspeed = tk.Entry(master=frm_info, width=10)
lbl_runspeed.grid(row=0, column=1,pady=10)
ent_runspeed.grid(row=0, column=2,pady=10)

lbl_rotations = tk.Label(master=frm_info, text = "# Rotations: ")
ent_rotations = tk.Entry(master=frm_info, width=10)
lbl_rotations.grid(row=1, column=1,pady=10)
ent_rotations.grid(row=1, column=2,pady=10)

var_direction = tk.IntVar()
check_direction = tk.Checkbutton(master=frm_info, text="Reverse", variable=var_direction)
check_direction.grid(row=3, column=2,padx=10,pady=10)

#Establish buttons
btn_go = tk.Button(master=frm_buttons, text = "GO", width = 10, height = 3, bg="green", command = rotate)

```

```

btn_stop = tk.Button(master=frm_buttons, text = "STOP", width = 10, height = 3, bg='red', command =
stopRotation)

btn_go.grid(row = 0, column = 1)
btn_stop.grid(row = 0, column = 2)

#Establish Output window
frm_output = tk.Frame(master = window)
frm_output.grid(row = 2, column = 0, sticky = "nesw", padx = 10, pady = 10)
outputwindow = tk.Text(master = frm_output, width = 50, height = 9)
outputwindow.pack()

# create instance of file like object
pl = PrintLogger(outputwindow)

#address digital channels
stepper0.setDeviceSerialNumber(130307)

#Assign event handlers
stepper0.setOnAttachHandler(onAttach)
stepper0.setOnDetachHandler(onDetach)

#Open and wait for attachment
if(stepper0.getAttached()):
    stepper0.close()
stepper0.openWaitForAttachment(3000)

#For degrees, = 360/(CPR*encoder res*gear ratio). I couldn't find the motor specs so I guessed. It's wrong by a
little.
stepper0.setRescaleFactor(360/(6475))
stepper0.setControlMode(StepperControlMode.CONTROL_MODE_RUN)

# replace sys.stdout with our object
default_stdout = sys.stdout
sys.stdout = pl

window.mainloop()

sys.stdout = default_stdout
#close channel
stopRotation()
stepper0.close()

```

A.2 PyInstaller Setup File

The following is a Python program I wrote to convert the GUI Python code into an executable file using PyInstaller. In writing I edited an example from the PyInstaller documentation. The Python code file's location is input, as well as options to make it a single file

which opens a windowed program. Running the file produces an EXE file, as well as a “build” folder which can be deleted.

```
# -*- coding: utf-8 -*-  
"""
```

```
Created on Tue Mar 23 13:08:28 2021
```

```
Short code to create EXE from python code, copied from PyInstaller documentation.
```

```
@author: Logan Page
```

```
"""
```

```
import PyInstaller.__main__
```

```
PyInstaller.__main__.run([  
    'C:\\Users\\DrAllredLab\\PhidgetGUI-Working.py',  
    '--onefile',  
    '--windowed'  
])
```

Index

alloy.....	2, 5, 6, 7, 8, 13, 16, 17, 19, 20, 27	Phidget	4, 21
EDX	4, 5, 11, 12, 15, 16	PyInstaller	4, 24
electron microscope	11, 15	Python	21, 24
ellipsometry.....	2, 7, 13, 14	self-healing.....	6
Kanaya-Okayama Range Equation	5, 13	silicon wafer	8, 13, 15, 16
logarithmic	2, 16, 17, 18, 20	sputtering.....	8, 9, 10, 11, 15, 16, 21
Los Alamos National Laboratory.....	2, 3, 7	stainless steel.....	6
niobium wire	10	stainless uranium.....	6, 20
nuclear power plants	6	target	5, 8, 9, 10
oxidation	2, 6, 8, 17, 20, 27	thickness.....	2, 10, 11, 15, 16, 17
passivation layer.....	2, 6, 7, 20	x ray	11, 13, 15
Passivation layer	6, 18, 20		

Bibliography

1. Idriss, H., *Surface reactions of uranium oxide powder, thin films and single crystals*. Surface Science Reports, 2010. **65**(3): p. 67-109.
2. McEachern, R.J. and P. Taylor, *A review of the oxidation of uranium dioxide at temperatures below 400 degrees C*. Journal of Nuclear Materials, 1998. **254**(2-3): p. 87-121.
3. Manner, W.L., et al., *An examination of the initial oxidation of a uranium-base alloy (U-14.1 at.% Nb) by O-2 and D2O using surface-sensitive techniques*. Applied Surface Science, 1999. 150(1-4): p. 73-88.
4. Fu, X.G., et al., *X-ray photoelectron spectroscopic study of the surface reaction of uranium-niobium alloy with O-2*. Surface Review and Letters, 2003. 10(2-3): p. 381-386.
5. Olsson, C.O.A. and D. Landolt, *Passive films on stainless steels - chemistry, structure and growth*. Electrochimica Acta, 2003. 48(9): p. 1093-1104.
6. Maurice, V. and P. Marcus, *Progress in corrosion science at atomic and nanometric scales*. Progress in Materials Science, 2018. 95: p. 132-171.
7. Knacke, O., O. Kubaschewski, and K. Hesselmann, *Thermochemical properties of inorganic substances*. 1991, Berlin; New York; Düsseldorf: Springer-Verlag ; Verlag Stahleisen.
8. Kelly, D., et al., *Surface characterization of oxidative corrosion of U-Nb alloys*. Journal of Vacuum Science & Technology a-Vacuum Surfaces and Films, 2001. 19(4): p. 1959-1964.
9. Embong, Z., et al., *In situ study of the initial stages of oxidation of alloy u-6wt.% nb with angle resolved x-ray photoelectron spectroscopy (ARXPS)*. Journal of Science and Technology, 2009. 1(1): p. 43-55.
10. Watkins, Erik B. et al., *Oxide structure of air-passivated U-6Nb alloy thin films*, Journal of Nuclear Materials, 2020.
11. Goldstein, Joseph, et al., *Scanning electron microscopy and x-ray microanalysis*. 2003, New York.